The final publication is available at Springer via http://dx.doi.org/10.1007/s10853-015-8873-8

Enhanced Ductility and Tensile Properties of Hybrid Montmorillonite/Cellulose Nanowhiskers Reinforced Polylactic Acid Nanocomposites

Reza Arjmandi[a], Azman Hassan[a]*, Stephen J. Eichhorn[b]*, M.K. Mohamad Haafiz[a, c], Zainoha Zakaria[d] and Faisal Amri Tanjung[a]

reza_arjmandiy@yahoo.com[a]; azmanh@cheme.utm.my[a*]; s.j.eichhorn@exeter.ac.uk[b*];

mhaafiz@usm.my[a, c]; zainoha@kimia.fs.utm.my[d]; icalamri@gmail.com[a]

[a]Department of Polymer Engineering, Faculty of Chemical Engineering, Universiti Teknologi Malaysia, 81310 Skudai UTM, Johor, Malaysia.

[b] College of Engineering, Maths & Physical Sciences, Physics Building, Stocker Road, University of Exeter, EX4 4QL, UK.

[c]School of Industrial Technology, Universiti Sains Malaysia, 11800 Penang, Malaysia.

[d]Faculty of Science, Universiti Teknologi Malaysia, UTM 81310, Skudai, Johor, Malaysia.

***Corresponding author:** Azman Hassan, Department of Polymer Engineering, Faculty of Chemical Engineering, Universiti Teknologi Malaysia, 81310 Skudai UTM, Johor, Malaysia. Tel.: +60 7 5537835; Fax: +60 7 5581 463. E-mail address: azmanh@cheme.utm.my; s.j.eichhorn@exeter.ac.uk.

Abstract

Montmorillonite (MMT)/cellulose nanowhiskers (CNW) reinforced polylactic acid (PLA) hybrid nanocomposites were prepared by solution casting. CNW were isolated from microcrystalline cellulose using a chemical swelling method. An initial study showed that the optimum MMT content, for mechanical properties, in a PLA/MMT nanocomposite is 5 phr. Various amounts of CNW were added to the optimum formulation of PLA/MMT to produce PLA/MMT/CNW hybrid nanocomposites. FT-IR analysis indicated the formation of some polar interactions, resulting in enhanced tensile properties of the hybrid nanocomposites. The highest tensile strength for the hybrid nanocomposites was obtained for a 1 phr CNW content. Young's modulus was also found to increase with an increasing CNW content. Interestingly, the strain to failure (or ductility) of the hybrid nanocomposites increased significantly from ~10 to ~90 % with the addition of 1 phr CNW. This increase in ductility was proposed to be due to the nucleation of crazes and the formation of shear bands in the PLA.

Keywords: Hybrid nanocomposites; cellulose nanowhiskers; montmorillonite; polylactic acid; tensile properties.

Introduction

In recent years, biodegradable polymers produced from renewable resources have become attractive for practical applications such as medical devices and food packaging [1]. Polylactic acid (PLA) is a biodegradable thermoplastic polyester produced from lactic acid and is derived by chemical synthesis or through the fermentation of sugar feed stocks, such as corn starch [2]. PLA is a ‘‘green polymer’’ because it can be finally degraded into CO_2 and H_2O [3]. PLA offers a potential alternative to petrochemical plastics in many applications, in part because of its high strength and stiffness and processability [4]. However, it has drawbacks such as low toughness, high production cost, brittleness, poor water vapour/gas barrier properties and undesirable thermal stability, making this bioplastic unsuitable for certain applications [5, 6]. Hence, many approaches have been adopted to overcome these inherent limitations, such as blending with other biodegradable polymers and also the development of composites and nanocomposites containing high aspect ratio organic and inorganic fillers [6, 7].

Polymer/clay nanocomposites have received significant attention compared to conventional composites because they often exhibit considerable improvement in mechanical, thermal, optical, physical properties and fire retardancy at low filler contents [8]. PLA/layered silicate nanocomposites have been shown to exhibit improved tensile strength and Young’s modulus compared to neat PLA [9]. Montmorillonite (MMT) has been the most commonly used layered silicate in this respect. Due to its hydrophilic character, MMT does not interact strongly with hydrophobic polymers such as PLA. For this reason, MMT must be modified by an organic reagent before it is used, which can strengthen the chemical interaction between PLA and MMT and also induces the formation of layered or exfoliated organic/inorganic nanocomposites [9]. MMT reinforced PLA nanocomposites can be prepared by two different methods; namely melt processing and solution casting techniques [9]. Based on previous studies, there is no clear optimum content for MMT-based nanocomposites. Thellen et al. [10] reported that an optimum tensile strength was achieved at a 5 wt.% MMT content, while He et al. [11] and Chang et al. [12] showed this occurred at 3 wt.% and 4 wt.% contents respectively. Young’s modulus has also been shown to increase gradually with an increase in the MMT content. However, these property enhancements are usually accompanied by a severe decrease in ductility. Therefore, there is a need to

investigate ways to produce PLA nanocomposites with both high strength/stiffness and ductility.

Cellulose is one of the most ubiquitous and abundant natural biopolymers and is also renewable and biodegradable. Most recently, cellulose nanofibres have been used as a reinforcing filler in polymeric matrix nanocomposites [13]. In terms of performance they possess high specific strength and modulus, easy processability and a relatively reactive surface. Cellulose fibres are also available from a wide variety of sources throughout the world [13, 14]. Cellulose nanowhiskers (CNW) have been gaining considerable interest among scientists during the last decade as potential nano-reinforcement in a number of different polymers. Tensile strength and Young's modulus of PLA nanocomposites have been shown to increase when CNW from grass were used as a reinforcement [15]. Additionally, CNW obtained from commercial MCC has been shown to improve the storage modulus of neat PLA [16]. Petersson et al. [7] reported that CNW improved the storage modulus of PLA at higher temperatures. A study to compare the effect of MMT and CNW on PLA was reported by Petersson and Oksman [2]. They found that MMT increased both tensile modulus and yield strength, while CNW only improved the yield strength. Petersson and Oksman [2] also reported that PLA/CNW nanocomposites have a higher ductility than PLA/MMT nanocomposites. This formed the basis to undertake the current study to determine the basis for the enhanced ductility of hybrid CNW/MMT filled PLA nanocomposites. Hybrid fillers can be promising for a number of applications where high strength/stiffness and ductility are required.

To the best of our knowledge, limited studies have been conducted on the use of MMT/CNW hybrid fillers in PLA polymer. Hong and Kim [8] showed that the simultaneous use of CNW and nanoclay as nanofillers improved the tensile strength and glass transition temperature of PLA using melt mixing. In the current study, the effects of CNW on mechanical and morphological properties of PLA/MMT/CNW hybrid nanocomposites prepared by solution casting have been investigated. The main reason for incorporation CNW into PLA/MMT nanocomposites is to increase ductility and Young's modulus of the nanocomposites which are important properties of packaging materials.

Materials and Methods

Materials

PLA (Nature Works TM PLA 300ID) in pellet form with a density of 1.24 g cm^{-3} and melt flow index (MFI) of *ca.* 15g $10min^{-1}$ (190°C $2.16kg^{-1}$) was obtained from Nature Works® LLC (Minnetonka, MN USA). MCC obtained from cotton linter with an average particle size of 50 μm was supplied by Sigma-Aldrich (Avicel; type PH-101). Organo-modified MMT (Nanomer 1.30TC) was obtained from Nanocor Inc. (Arlington Heights IL, USA). Nanomer 1.30TC is organically modified with approximately 30 wt.% of octadecylamine and has a mean dry particle size of 16-22 mm. Chloroform, *N, N*-dimethylacetamide (DMAc) (99 % purity) and lithium chloride (LiCl) (99 % Purity) were purchased from Merck, Malaysia.

Preparation of CNW

Chemical swelling

As described by Oksman et al. [5] and Pereda et al. [17], CNW were prepared by swelling MCC and separating to whiskers by a sequence of chemical and ultrasonification treatments using DMAc and 0.5 % LiCl solution as swelling agents. The initial concentration of MCC in DMAc/LiCl was 10 wt.%. Then, MCC was vigorously agitated using a mechanical stirrer inside a water bath at 70 °C for 12 h to swell the MCC particles. Subsequently, the slightly swelled particles were sonified using an ultrasonic bath (Branson 2510) for 3 h over a period of 5 days with long intervals between each sonification treatment to separate the CNW. The gel-like suspension of CNW were repeatedly washed with distilled water, then freeze-dried and designated as CNW.

Preparation of PLA

Firstly, 10 g PLA pellets were fully dissolved in 64 ml of chloroform by heating in a water bath at 60 °C for 2 h with constant stirring, as described by Sanchez-Garcia and Lagaron [6]. Subsequently, the PLA solution was immediately cast onto clean glass plates and the solvent was left to evaporate at room temperature for 48 h. The thickness of the resulting cast film was approximately 100 μm.

Preparation of PLA/MMT nanocomposites

PLA/MMT nanocomposites were prepared by mixing 10 g of PLA pellets with MMT at different contents (1, 3, 5, 7 and 9 phr). The various PLA/MMT mixtures were placed in 64 ml of chloroform and stirred with vigorous agitation for 2 h at 60 °C until the PLA pellets were completely dissolved. The suspensions were then sonified for 5 min and immediately cast onto a clean glass plate to obtain nanocomposite films with ~100 μm thickness. The nanocomposites with MMT contents of 1, 3, 5, 7 and 9 phr were designated as P/M1, P/M3, P/M5, P/M7 and P/M9, respectively. Table 1 presents the formulation of PLA nanocomposites with various MMT contents.

Preparation of PLA/CNW nanocomposites

PLA/CNW nanocomposites were prepared by mixing 10 g of PLA pellets with CNW at different contents (1, 3, 5, 7 and 9 phr). The CNW nanofiller used was in water suspension form. Solvent exchange was then carried out via centrifugation using a Universal 32 Hettich centrifuge (Newport Pagnell, England). Water was then exchanged with acetone and acetone exchanged with chloroform. The CNW filler was then sonified using an ultrasonic bath (Branson 2510) for 5 minutes to ensure a homogenous dispersion inside the chloroform. The dispersed CNW was then transferred into a PLA flask. Subsequently, the various PLA/CNW mixtures were placed in 64 ml of chloroform and stirred with vigorous agitation for 2 h at 60 °C until the PLA pellets were completely dissolved. The suspensions were then sonified for 5 min and immediately cast onto a clean glass plate to obtain nanocomposite films with ~100 μm thickness. The nanocomposites were designated as P/C1, P/C3, P/C5, P/C7 and P/C9, respectively (Table 1).

Preparation of PLA/MMT/CNW hybrid nanocomposites

The PLA/MMT/CNW hybrid nanocomposites were prepared by mixing 10 g of PLA pellets with 5 phr of MMT and different contents of CNW (1, 3, 5, 7 and 9 phr). The CNW nanofiller used in this preparation step was the same that was used to produce the PLA/CNW nanocomposites. Therefore, the dispersed CNW was transferred into PLA with 5 phr MMT. Subsequently, the various PLA/MMT/CNW mixtures were placed in 64 ml of chloroform and stirred with vigorous agitation for 2 hours at 60 °C until the PLA pellets were dissolved.

The dissolved PLA containing MMT/CNW was then sonified for another 5 minutes. Finally, the solution was immediately cast onto a clean glass plate to obtain nanocomposite films that were ~100 μm thick. The hybrid nanocomposites were designated as P/M5/C1, P/M5/C3, P/M5/C5, P/M5/C7 and P/M5/C9 (Table 1).

Characterization

Fourier transform infrared spectroscopy

Fourier transform infrared spectroscopy (FT-IR) was performed using a Perkin Elmer 1600 Infrared spectrometer. FT-IR spectra of the samples were recorded using Nicolet's AVATAR 360 at 32 scans with a resolution of 4 cm^{-1} and within the wavenumber range of 370 to 4000 cm^{-1}.

Tensile testing

Tensile testing was performed on an Instron 4400 Universal Tester. The tensile tests were carried out at room temperature according to the ASTM D882 type V standard. A fixed crosshead speed of 12.5 mm min^{-1} was utilized in all cases, and mean data were taken as an average from 10 tests.

Morphology analysis

Sample morphologies were characterized by light microscopy, field emission scanning electron microscopy (FESEM), transmission electron microscopy (TEM) and atomic force microscopy (AFM). Light microscopy was performed using an Olympus SZX9 stereomicroscope system. FESEM was conducted on a Carl Zeiss (Germany) Supra 35 VP microscope using an accelerating voltage in the range 8–10 kV. The samples were sputter-coated with gold prior to observation. The microstructure of PLA nanocomposites and the filler dispersion in the matrix were investigated using a TEM (JEOL JEM-2010). TEM samples were sectioned with an ultra-microtome (RMC, model MTXL) to obtain ~70 nm thick slices. AFM analysis was performed using an SPA-300HV atomic force microscope with a SPI 3800 controller. The neat PLA and nanocomposites samples (0.1 mm × 0.1 mm) were analysed directly.

X-ray diffraction

X-ray diffraction (XRD) was performed on a Siemens (Berlin, Germany) D5000 X-ray diffractometer. The diffraction patterns were recorded using a step size of 0.02°, from 2θ = 2.0 to 10.0°. The interlayer distances (*d*-spacing) of the MMT in the nanocomposites were derived from the peak positions in the XRD patterns, according to Bragg's Law.

$$d\text{-spacing} = n\lambda / \sin\theta_p \qquad (1)$$

where *n* is an integer, θ_p is the diffraction angle giving the primary diffraction peak and λ is the X-ray wavelength. In these experiments, λ= 0.15406 nm (Cu Kα) and n = 1 were used.

Results and Discussion

FT-IR spectroscopy analysis

Figs. 1a-d illustrate typical IR spectra of neat PLA, a P/M5 nanocomposite, a P/C3 nanocomposite and a P/M5/C1 hybrid nanocomposite, respectively. As shown in Fig. 1a, the peaks at 1049 and 1457 cm^{-1} correspond to –OH and $–CH_3$ bending vibrations, the peak at 1089 cm^{-1} is assigned to the stretching vibration of C-O groups and the peak at 1764 cm^{-1} is attributed to the stretching vibration of C=O groups. The absorption peaks at 2948 and 2997 cm^{-1} are attributed to an asymmetrical stretching vibration of a –CH moiety, and the peaks at 3508 and 3644 cm^{-1} correspond to a bending vibration of two terminal hydroxyl groups [18].

Upon the addition of the MMT into the PLA (Fig. 1b), the absorption peaks at 1089, 1764 and 3508 cm^{-1} of the PLA shifted to lower wave number positions of (1082, 1756 and 3502 cm^{-1}, respectively). Moreover, two new peaks appeared at 465 and 520 cm^{-1} that correspond to stretching vibrations of the Si–O groups of the MMT filler. These changes in the spectra are thought to be due to a good interaction between the PLA and the MMT filler via the formation of polar interactions between the functional groups of both components [19]. It is noticeable that the MMT contains a large number of polar sites distributed uniformly along the body structure, indicating an electron density content around the surfaces and interlayer spaces. As a result, some polar interaction between the PLA and the MMT filler are thought to readily occur. Liu et al. [20] indicated that the shifting of absorption peaks in the IR spectrum of PLA nanocomposites could be due to the formation of polar interactions between the hydroxyl groups of the PLA and the Si–O groups of the MMT.

As shown in Fig. 1c, a new absorption peak at 3851 cm^{-1} was observed in the IR spectrum of the P/C3 nanocomposite, which corresponds to a bending vibration of the hydroxyl groups of the CNW and PLA. The peaks located at 1089 cm^{-1}, 1764 cm^{-1} and 3508 cm^{-1} in the PLA spectrum shifted to lower wave number positions (1080, 1754 and 3498 cm^{-1}, respectively). These peak shifts indicate a good interaction between the hydroxyl/carbonyl groups of the PLA and the hydroxyl groups of the CNW. Furthermore, the effect of the addition of CNW on the PLA/MMT nanocomposites is shown in Fig. 1d. A new absorption peak at 3851 cm^{-1} was also observed in the P/M5/C1 IR spectrum (Fig. 1d) compared to the P/M5 nanocomposite. The shift of the peak from 3644 to 3651 cm^{-1} was also observed indicating a good interaction between the hydroxyl group of the CNW and the hydroxyl/carbonyl group of the PLA. Meanwhile, the presence of a peak at 3851 cm^{-1} assigned to a bending vibration of the hydroxyl groups decorating the CNW on the PLA contributed to the increased hydrophilic character of the hybrid nanocomposites. Interestingly, the peak that shifted to 3851 cm^{-1} becomes broader compared to the same peak for the P/C3 nanocomposites. It is thought that this broadening is evidence of polar interactions [21]. These findings clearly imply that either the addition of a single filler or the addition of both MMT and CNW fillers has changed the molecular conformation of the PLA, thus altering the properties of the nanocomposites.

Tensile properties

Typical stress–strain curves of neat PLA and P/M5, P/C3 and P/M5/C1 nanocomposites are shown in Fig.2. As can be clearly seen from Fig.2, the tensile strength of P/M5/C1 hybrid nanocomposite increased compared to nanocomposites with a single filler and neat PLA. An interesting observation from Fig. 2 is that the elongation at break also increased in the hybrid sample compared to P/M5 and P/C3 nanocomposites.

Figs. 3a-c report the tensile strength and Young's modulus of PLA/MMT and PLA/CNW nanocomposites and PLA/MMT/CNW hybrid nanocomposites, respectively. Fig. 3a presents the tensile strengths and Young's modulus of the PLA and the PLA/MMT nanocomposites at various MMT contents. The tensile strength of the PLA/MMT nanocomposites is observed to increase with the addition of MMT, reaching a plateau at a filler content of 5 phr, then declining at higher contents. The tensile strength of PLA/MMT

nanocomposites at a 5 phr filler content is ~63 % higher than that of the neat PLA, suggesting a significant reinforcing effect of the inorganic phase. It is thought that at this filler content the MMT is distributed uniformly within the PLA leading to the formation of sufficient percolation networks. As a result, at this filler content, the tensile strength reaches a maximum value. However, when the filler content exceeds 5 phr, the tensile strength dramatically decreases probably due to the aggregation of the filler resulting in stress concentration points for fracture. This result is in agreement with Lee et al. [22], where the agglomeration of MMT at filler contents >5 wt.% resulted in a decrease in tensile strength. Young's modulus of PLA/MMT nanocomposites however increased steeply with increasing MMT filler content. It is notable that Young's modulus of PLA/MMT nanocomposites increased by ~18 %, compared to neat PLA film. This increase is attributed to the rigid MMT fillers which constrict segmental chain motion in the polymer matrix, which is consistent with a previous report [11].

Fig. 3b presents the tensile strengths and Young's modulus of the PLA/CNW nanocomposites at various CNW contents. The tensile strength is observed to increase with the addition of CNW and reaches a maximum tensile strength at 3 phr, subsequently decreasing at higher filler contents. The tensile strength of PLA/CNW nanocomposites at 3 phr filler content is ~71 % higher than the neat PLA suggesting a good dispersion and interaction between the –OH groups of the CNW and the –OH/C=O groups of the PLA. At this filler content the CNW are thought to be distributed uniformly within the PLA leading to an increase in filler-matrix interactions increase resulting in an improved tensile strength. Similar conclusions were previously reported by Baheti et al. [23] and Bras et al. [24]. However, when the filler content >3 phr, the tensile strength decreased. This decrease is probably due to aggregation of the CNW in the PLA, which then act as stress concentration points. Similar observations were reported by Liu et al. [20] and Baheti et al. [23] when PLA was reinforced using halloysite and jute nanofibres, respectively. Young's modulus of PLA/CNW nanocomposites however increased gradually with an increase in the CNW filler content (Fig. 3b); Young's modulus of PLA/CNW nanocomposites increased by ~25 % compared to neat PLA. This increase was attributed to the stiffening effect of the high modulus CNW reinforcement. Similar results were reported by Cheng et al. [25].

Fig. 3c presents the effect of CNW content on the tensile strength and Young's modulus of PLA/MMT/CNW hybrid nanocomposites. It was observed that these hybrid nanocomposites (at a 1 phr CNW content) had the highest tensile strengths; increases of ~27, ~21 and ~106 % were observed compared to those of the P/M5 and P/C3 nanocomposites and neat PLA, respectively. The highest tensile strength at 1 phr CNW content might be attributed to the homogeneous dispersion and specific interaction that took place between the PLA and both MMT and CNW. This also indicates a positive synergistic effect of MMT and CNW in the enhancement of the tensile strength of the hybrid nanocomposites through the formation of good interactions with the PLA. Similar conclusion have observed by Wang et al. [26] with CNW reinforced PLA nanocomposites. When the CNW content was increased beyond 1 phr the tensile strength however decreased. The decrease in tensile strength is thought to be due to the aggregation of MMT platelets induced by van der Waal's forces and thereby a reduced surface area of interaction between the PLA and both MMT and CNW. This result is in agreement with Liu et al. [20] for a halloysite filled PLA polymer. Young's modulus of PLA/MMT/CNW hybrid nanocomposites (Fig. 3c) gradually increased from 4.8 to 5.5 GPa with an increase in the CNW content. With the addition of CNW at 1, 5 and 9 phr, Young's modulus of the hybrid nanocomposites increased by ~23, ~27 and ~31 % above that of the neat PLA, respectively. It is expected that the high modulus of both MMT and CNW play a vital role in the improvement of Young's modulus of the hybrid nanocomposites. Similar conclusions were reported by Cheng et al. [25] and Haafiz et al. [27], when PLA was reinforced with cellulose fibres and microcrystalline cellulose, respectively.

The hybrid nanocomposites were however observed to have higher elongation at break as compared with the non-hybridized samples. Table 2 summarizes the elongation at break of PLA/MMT nanocomposites, PLA/CNW nanocomposites and PLA/MMT/CNW hybrid nanocomposites. The addition of 1 phr CNW filler into the PLA matrix remarkably increased the strain to failure (or ductility) of the nanocomposites; the elongation at break of P/C1 nanocomposites increased from ~10 to ~69 % compared to the optimum formulation of PLA/MMT. However, the elongation at break decreased with any further increase in CNW filler content. The addition of 1 phr CNW filler into the P/M5 nanocomposite in order to produce P/M5/C1 hybrid nanocomposite significantly increased strain to failure of the hybrid nanocomposites compared to the P/M5 sample (from ~10 to ~90 %). However, again the

strain to failure decreased with any further addition of CNW. The initial increase in strain to failure of the hybrid nanocomposites could be attributed to CNW reducing the ability of MMT to restrict the mobility of polymer chains. However, the addition of a similar amount of CNW increased the tensile strength as well due to the good adhesion of CNW to PLA. Additionally, this result seemed likely to be due to their enhanced hydrophilic character as confirmed by the FT-IR analysis. Thus, the existence of a proportional content of hydrophilic groups may contribute to plasticization leading to enhanced deformability. It may also be the case that the addition of CNW leads to nucleation of crazes in the amorphous fraction of the PLA resin, as has been previously observed for a different system [28]. In addition, Fig. 4a-f shows typical images of the test specimens of a P/M5 nanocomposite film, a P/C1 nanocomposite film and a P/M5/C1 hybrid nanocomposite film before and after deformation. According to Bulota and Hughes [28], the high strain-to-failure arising from craze nucleation is indicated by a whitening of the polymer matrix due to air scattering. As can be clearly observed from Fig. 4f, P/M5/C1 hybrid nanocomposites exhibit much greater ductility compared to all other specimens with a single filler component, accompanied by pronounced stress whitening. Additionally, the stress-whitened zone observed in the test specimens suggests the presence of shear bands in the PLA. Furthermore, the tensile strength and elongation at break of P/M5/C1 hybrid nanocomposite increased compared to nanocomposites with the single filler, as confirmed earlier by typical stress–strain curves. This result suggests that CNW might nucleate crazes, possibly due to their high surface to volume ratio.

Light microscopy

Further evidence of crazing and shear banding in the samples was obtained using light microscopy. Figs. 5a and b report typical light microscope images from a P/M5/C1 hybrid nanocomposites before and after deformation, respectively. To better observe the crazes and shear bands, light microscopy images were conducted using back-illumination. Fig. 5b, clearly shows crazes forming in the sample, which look like cracks but characteristically form perpendicular to the draw direction. In addition, the formation of shear bands (at 45° to the direction orthogonal to the tensile axis) were also clearly observed (see Fig. 5b). These shear bands may also increase the toughness of the nanocomposites through localised

yielding of the polymer. High strain within a craze zone and the formation of shear bands could result in an overall increase in the strain to failure of the sample.

Field emission scanning electron microscopy

Figs. 6a-e shows field emission scanning electron microscopy (FESEM) images of the fractured cross-sectional surfaces of neat PLA, PLA/MMT nanocomposites, PLA/CNW nanocomposites and PLA/MMT/CNW hybrid nanocomposites. Fig. 6a, shows that neat PLA has a typically smooth fracture surface [29]. Fig. 6b presents the typical fractured cross-sectional surfaces of P/M5 nanocomposites. It can be seen from Fig. 6b that MMT disperses uniformly throughout the PLA due to its finer particle size. On the other hand, the fracture of PLA/CNW displayed different behaviour compared to the neat PLA. Typical fractured cross-sectional surfaces of P/C3 nanocomposites are shown in Fig. 6c. It can be clearly seen that CNW is distributed uniformly within the PLA matrix. Similar observations were reported by Sanchez-Garcia and Lagaron [6], with CNW reinforced PLA nanocomposites. The white dot that appeared on the surface of the cross section could be attributed to the perpendicular plane of the CNW. Similar observations were reported by Roohani et al. [30], for CNW reinforced polyvinyl alcohol nanocomposites. Fig. 6d show typical fractured cross-sectional surfaces of P/M5/C1 hybrid nanocomposites. CNW disperses uniformly throughout the PLA; MMT fillers are indicated by the white arrow and the CNW particles by the red arrows. Accordingly, the interaction between the matrix and the fillers has enhanced considerably, as reflected by an increased tensile strength. Meanwhile, at higher filler content filler-filler interactions are more favourable than filler-matrix interactions, leading to filler agglomeration (Fig. 6e). From Fig. 6e, agglomeration of the MMT filler (circled area) and the CNW particles (red arrows) in a P/M5/C3 hybrid nanocomposite can be seen. This agglomeration plays a major role in the decreasing the tensile strength of the hybrid nanocomposites.

Transmission electron microscopy

Transmission electron microscopy (TEM) micrographs of the neat PLA, diluted water suspension of CNW, a P/M5 nanocomposite and a P/M5/C1 hybrid nanocomposites are shown in Figs. 7a-d, respectively. The TEM micrograph of neat PLA (Fig. 7a) clearly

displays a smooth and clean surface, with no obvious features. The nanofillers can be observed in the PLA matrix for the nanocomposite samples. As can be seen in Fig. 7b, a diluted water suspension of CNW was imaged using TEM; this image shows CNWs with nanometer length scales. However, some clustering is noted of the CNWs, which may be due to a lack of charge at their surface. A typical TEM micrograph of P/M5 nanocomposite is displayed in Fig. 7c. As can be seen the multilayer of MMT fillers is intercalated in the PLA, whereas the spaces between the dark lines are the interlayer spaces (white arrow). Similar observations were reported for PLA reinforced with MMT filler [12, 31]. The silicate-layered MMT evenly disperses throughout the PLA (white arrow), while nanorod-like structures corresponding to the CNW filler also uniformly disperses in the PLA (red arrow; Fig. 7d). The good dispersion of MMT and CNW could be the reason for tensile strength improvements as previously discussed. Additionally, it is speculated that given the evidence presented in Fig. 7d that the CNWs bind closely to the clay particles, increasing the available surface area for interaction with the PLA matrix. This effect could further enhance the stiffness of the nanocomposites. This finding indicates that the presence of a high content of CNW may induce the agglomeration of MMT filler and adversely affect the intercalation process of the MMT, leading to a decrease in the tensile strength.

Atomic Force Microscopy

To further explore the dispersion behaviour of the MMT and CNW fillers inside the PLA matrix, PLA/MMT nanocomposites and PLA/MMT/CNW hybrid nanocomposites were observed using atomic force microscopy (AFM). Figs. 8a-h shows typical AFM micrographs of neat PLA, a P/M5 nanocomposite and a P/M5/C1 hybrid nanocomposite. It can clearly be seen that the neat PLA has a smooth surface topography which is typical for an unfilled matrix material (Figs. 8a and b). With the incorporation of the MMT filler and both MMT/CNW fillers the surface topography of the neat PLA becomes rough, owing to uneven filler dispersion within the matrix (Figs. 8c-h). From Fig. 8c, the P/M5 nanocomposites show a topography corresponding to the intercalated MMT filler in the PLA. Individual layers of the MMT cannot be discerned, but a striated structure of the layered MMT can be deduced from the images, as indicated by a circle (Figs. 8d and e). This result is in agreement with Becker et al. [32]. On the other hand, the P/M5/C1 hybrid

nanocomposite exhibits a fibrous-structured topography with the presence of the CNW filler (Figs. 8f-h). Both MMT and CNW fillers are observed to be dispersed uniformly within the PLA matrix (Fig. 8g). The nanorod-like nature of the CNW filler distributed within the PLA can be seen (indicated by an arrow) and the striated structure of MMT layered in the PLA matrix (indicated by circle). This nanorod-like fibre of the CNW and striated structure of the layered MMT can also be seen in Fig. 8h.

X-ray diffraction

In order to better confirm the existence of the interaction between the fillers and the matrix, X-ray diffraction (XRD) analysis of the nanocomposites was carried out. X-ray diffraction (XRD) patterns of PLA, MMT, a P/M5 nanocomposite, a P/M5/C1 and a P/M5/C3 hybrid nanocomposites are shown in Fig. 9. Table 3 tabulates the relative *d*-spacings of the nanocomposites. The MMT filler exhibits a diffraction peak at $2\theta = 4.15°$, corresponding to the 001 lattice plane with a *d*-spacing of 2.14 nm. This peak shifts to a lower 2θ value as the MMT filler is incorporated into the PLA; the peak shifted to $2\theta = 2.82°$ with *d*-spacing of 3.15 nm. This result indicates the scattering an intercalation of the mineral phase by the PLA resin [2, 33]. Moreover, this intercalation in the interlayer spacing of the MMT may be due to the formation of interactions with the PLA, thus providing the possibility for PLA chains to diffuse between the gallery layers of the MMT during processing [34]. This diffusion of PLA chains in the MMT layers would be expected to increase the inter-gallery distance and reduce the electrostatic attraction between adjacent platelets [34]. Petersson and Oksman [2] reported that the a distribution of MMT in the PLA matrix was due to interactions between ammonium groups in the surfactant of organically modified MMT with the carbonyl group of PLA chain segments, leading to MMT intercalation. Other possible interactions between the PLA and the MMT filler may also occur via the hydroxyl groups of the PLA and hydroxyl groups on the MMT [29].

The XRD patterns of the PLA hybrid nanocomposites with 5 phr of MMT and 1 phr of CNW displayed a slight increase in *d*-spacing for the (001) lattice plane as compared to that of a P/M5 nanocomposite (Table 3). This increase is an indication of a further enlarged interlayer space in the MMT nanostructure that could be due to the chain conformation of the matrix caused by a synergistic interaction with the CNW. However, a higher content of

the CNW results a slight decrease in the *d*-spacing and the intensity of the 001 crystal peak compared to the P/M5/C1 hybrid nanocomposite (Table 3). This effect is thought to be due to the aggregation of the MMT filler and the reduced surface area of interaction between the PLA and both fillers. It is also thought that this decrease in *d*-spacing contributes to a decrease in the tensile strength for the hybrid nanocomposites with a CNW content higher than 1 phr. In general, the mechanical data, FESEM and TEM micrographs of the nanocomposites and hybrid nanocomposites correlated well with the XRD results.

Conclusion

PLA/MMT and CNW nanocomposites were prepared by solution casting. FT-IR analysis showed that some polar interactions occurred between the PLA and the both fillers. The tensile strength of PLA/MMT nanocomposites increased with the addition of MMT and reached a maximum value at 5 phr. In addition, the tensile strength of PLA/CNW nanocomposites increased with CNW content and reached a maximum value at a 3 phr CNW content. The tensile strength of hybrid nanocomposites also increased significantly by adding 1 phr of CNW to an optimum formulation for a PLA/MMT nanocomposite. Furthermore, the Young's modulus of PLA/MMT, PLA/CNW and PLA/MMT/CNW nanocomposites increased steadily with the addition of MMT, CNW and hybrid fillers, respectively. Due to the possible nucleation of crazes in the amorphous fraction of the PLA and the formation of shear bands, the ductility of PLA/MMT/CNW hybrid nanocomposites increased significantly compared to PLA/MMT and PLA/CNW nanocomposites. The formation of an intercalated nanostructure in PLA/MMT nanocomposites and PLA/MMT/CNW hybrid nanocomposites was confirmed by TEM and XRD analysis. The dispersed MMT filler contributed to the increased tensile properties of the PLA/MMT nanocomposites. However, a uniform dispersion of CNW was readily apparent with the addition of 1 phr CNW in the P/M5 nanocomposite. Due to the presence of dispersed CNW in the PLA/MMT/CNW hybrid nanocomposites, the interlayer spacing of the MMT slightly increased, leading to more intercalation, which in turn increased the tensile strength of the hybrid nanocomposites. The remaining challenge is to find an effective method to further enhance adhesion between PLA and both MMT and CNW. Overcoming this challenge is expected to further enhance the ductility, Young's modulus and tensile properties of these interesting materials.

Acknowledgement

Authors wish to acknowledge the Universiti Teknologi Malaysia (UTM) and Research University Grant 05H22, sub-code: Q.J130000.2509.05H22 for financial support.

References

[1] Vroman I and Tighzert L (2009) Biodegradable polymers, Materials 2:307-344.

[2] Petersson L snd Oksman K (2006) Biopolymer based nanocomposites: comparing layered silicates and microcrystalline cellulose as nanoreinforcement, Compos Sci Technol 66:2187–2196.

[3] Liu R, Luo S, Cao J, Peng Y (2013) Characterization of organo-montmorillonite (OMMT) modified wood flour and properties of its composites with poly (lactic acid), Compos Part A Appl Sci Manuf 51:33-42.

[4] Huda MS, Drzal LT, Mohanty AK, Misra M (2008) Effect of fiber surface-treatments on the properties of laminated biocomposites from poly (lactic acid) (PLA) and kenaf fibers, Compos Sci Technol 68:424-432.

[5] Oksman K, Mathew AP, Bondeson D, Kvien I (2006) Manufacturing process of cellulose whiskers/polylactic acid nanocomposites, Compos Sci Technol 66:2776-2784.

[6] Sanchez-Garcia MD and Lagaron JM (2010) On the use of plant cellulose nanowhiskers to enhance the barrier properties of polylactic acid, Cellulose 17:987-1004.

[7] Petersson L, Kvien I, Oksman K (2007) Structure and thermal properties of poly (lactic acid)/cellulose whiskers nanocomposite materials, Compos Sci Technol 67:2535–2544.

[8] Hong J and Kim DS (2013) Preparation and physical properties of polylactide/cellulose nanowhisker/nanoclay composites, Polym Compos 34:293-298.

[9] Sinha Ray S and Okamoto M (2003) Polymer/layered silicate nanocomposites: A review from preparation to processing. Prog Polym Sci 28:1539–1641.

[10] Thellen C, Orroth C, Froio D, Ziegler D, Lucciarini J, Farrell R, Ratto JA (2005) Influence of montmorillonite layered silicate on plasticized poly (L-lactide) blown films, Polymer 46:11716-11727.

[11] He YN, Guo K, Chen JZ, Niu MJ, Wang WJ, Li XF (2011) Preparation and Characterization of Poly(lactic acid)/Montmorillonite Nanocomposites via a Masterbatching Method, Adv Mat Res 335-336:1493-1498.

[12] Chang JH, An YU, Sur GS (2003) Poly(lactic acid) Nanocomposites with Various Organoclays. I. Thermomechanical Properties, Morphology, and Gas Permeability, J Polym Sci B Polym Phys 41:94–103.

[13] Azizi Samir MAS, Alloin F, Dufresne A (2005) Review of recent research into cellulosic whiskers, their properties and their application in nanocomposite field, Biomacromolecules 6:612-626.

[14] Li R, Fei J, Cai Y, Li Y, Feng J, Yao J (2009) Cellulose whiskers extracted from mulberry: a novel biomass production, Carbohydr Polym 76:94-99.

[15] Pandey JK, Chu WS, Kim CS, Lee CS, Ahn SHM (2009) Bio-nano reinforcement of environmentally degradable polymer matrix by cellulose whiskers from grass, Compos Part B Eng 40:676-680.

[16] Cho SY, Park HH, Yun YS, Jin HJ (2013) Cellulose nanowhisker-incorporated poly (lactic acid) composites for high thermal stability, Fiber Polym 14:1001-1005.

[17] Pereda M, Amica G, Rácz I, Marcovich NE (2011) Structure and properties of nanocomposite films based on sodium caseinate and nanocellulose fibers, J Food Eng 103:76-83.

[18] Field LD, Sternhell S, Kalman JR (2012) Organic structures from spectra 5th edn. John Wiley & Sons.

[19] Chen NL, Feng HX, Guo JW, Luo HM, Qiu JH (2011) Biodegradable Poly(lactic acid)/TDI-montmorillonite Nanocomposites: Preparation and Characterization, Adv Mat Res 221:211-215.

[20] Liu M, Zhang Y, Zhou C (2013) Nanocomposites of halloysite and polylactide, Appl Clay Sci 75-76:52-59.

[21] Qu P, Gao Y, Wu G, Zhang L (2010) Nanocomposite of Poly(Lactid Acid) reinforced with cellulose nanofibrils, BioResources 5:1811-1823.

[22] Lee J, Sun Q, Deng Y (2008) Nanocomposites from regenerated cellulose and nanoclay, J Biobased Mater Bio 2:162–168.

[23] Baheti V, Militky J, Marsalkova M (2013) Mechanical properties of poly lactic acid composite films reinforced with wet milled jute nanofibers, Polym Compos 34:2133-2141.

[24] Bras J, Hassan ML, Bruzesse C, Hassan EA, El-Wakil NA, Dufresne, A (2010) Mechanical, barrier, and biodegradability properties of bagasse cellulose whiskers reinforced natural rubber nanocomposites, Ind Crop Prod 32:627-633.

[25] Cheng Q, Wang S, Rials TG (2009) Poly (vinyl alcohol) nanocomposites reinforced with cellulose fibrils isolated by high intensity ultrasonication, Compos Part A Appl Sci Manuf 40:218-224.

[26] Wang Y, Cao X, Zhang L (2006) Effects of cellulose whiskers on properties of soy protein thermoplastics, Macromol Biosci 6:524-531.

[27] Haafiz MKM, Hassan A, Zakaria Z, Inuwaa IM, Islam MS, Jawaid M (2013) Properties of polylactic acid composites reinforced with oil palm biomass microcrystalline cellulose, Carbohydr Polym 98:139-145.

[28] Bulota M and Hughes M (2012) Toughening mechanisms in poly(lactic) acid reinforced with TEMPO-oxidized cellulose, J Mater Sci 47:5517-5523.

[29] Jiang L, Zhang J, Wolcott MP (2007) Comparison of polylactide/nanosized calcium carbonate and polylactide/montmorillonite composites: Reinforcing effects and toughening mechanisms, Polymer 48:7632–7644.

[30] Roohani M, Habibi Y, Belgacem NM, Ebrahim G, Karimi AN, Dufresne A (2008) Cellulose whiskers reinforced polyvinyl alcohol copolymers nanocomposites, Eur Polym J 44:2489-2498.

[31] Chang JH, An YU, Cho D, Giannelis EP (2003) Poly(lactic acid) nanocomposites: comparison of their properties with montmorillonite and synthetic mica (II), Polymer 44:3715-3720.

[32] Becker O, Varley R, Simon G (2002) Morphology, thermal relaxations and mechanical properties of layered silicate nanocomposites based upon high-functionality epoxy resins, Polymer 43:4365-4373.

[33] Shyang CW, Kuen LS (2008) Flexural, morphological and thermal properties of poly(lactic acid)/organo-montmorillonite nanocomposites, Polym Polym Compos 16:263-270.

[34] Balakrishnan H, Hassan A, Wahit MU, Yussuf AA, Razak SBA (2010) Novel toughened polylactic acid nanocomposite: Mechanical, thermal and morphological properties, Mater Design 31:3289-3298.

Figure caption

Fig. 1 Typical FT-IR spectra of (a) neat PLA, (b) a P/M5 nanocomposite, (c) a P/C3 nanocomposite and (d) a P/M5/C1 hybrid nanocomposite

Fig. 2 Typical stress-strain curves of neat PLA, a P/M5 nanocomposite, a P/C3 nanocomposite and a P/M5/C1 hybrid nanocomposite

Fig. 3 Tensile strength and Young's modulus of (a) PLA/MMT nanocomposites, (b) PLA/CNW nanocomposite and (c) PLA/MMT/CNW hybrid nanocomposites. Errors presented represent standard deviations from the mean (n = 10)

Fig. 4 Typical images of the test specimens. (a) a P/M5 nanocomposite film prior deformation, (b) a P/M5 nanocomposite film at ~10 % strain, (c) a P/C1 nanocomposite film prior deformation, (d) a P/C1 nanocomposite film at ~69 % strain, (e) a P/M5/C1 hybrid nanocomposite film prior deformation and (f) a P/M5/C1 hybrid nanocomposite film at ~90 % strain

Fig. 5 Typical light microscopy images of a P/M5/C1 hybrid nanocomposite film (a) prior deformation and (b) after deformation

Fig. 6 FESEM micrographs of fractured cross-sections of (a) neat PLA, (b) a P/M5 nanocomposite, (c) a P/C3 nanocomposite, (d) a P/M5/C1 hybrid nanocomposite and (e) a P/M5/C3 hybrid nanocomposite. MMT fillers are indicated by the white arrow, the CNW particles are indicated by a red arrow and the agglomerated MMT platelets are indicated by a circle

Fig. 7 TEM micrographs of (a) neat PLA, (b) a deposited diluted water suspension of CNW, (c) a P/M5 nanocomposite and (d) a P/M5/C1 hybrid nanocomposite. MMT fillers are indicated by the white arrows and the CNW particles by the red arrows

Fig. 8 AFM images, (a and b) topography and deflection images of neat PLA, (c, d and e) topography, deflection and corresponding magnified images of P/M5 nanocomposites, (f, g and h) topography, deflection and corresponding magnified images of P/M5/C1 hybrid nanocomposites, respectively

Fig. 9 XRD pattern of neat PLA, MMT, a P/M5 nanocomposite, a P/M5/C1 hybrid nanocomposite and a P/M5/C3 hybrid nanocomposite

Table 1 Polylactic acid nanocomposites formulation.

Designation	PLA (wt.%)	MMT (phr)	CNW (phr)
PLA	100	0	0
P/M1	100	1	0
P/M3	100	3	0
P/M5	100	5	0
P/M7	100	7	0
P/M9	100	9	0
P/C1	100	0	1
P/C3	100	0	3
P/C5	100	0	5
P/C7	100	0	7
P/C9	100	0	9
P/M5/C1	100	5	1
P/M5/C3	100	5	3
P/M5/C5	100	5	5
P/M5/C7	100	5	7
P/M5/C9	100	5	9

phr = parts per hundred parts of polymer (PLA).

Table 2 Elongation at break of (a) PLA/MMT nanocomposites, (b) PLA/CNW nanocomposites and (c) PLA/MMT/CNW hybrid nanocomposites.

	Designation	Elongation at break (%)
(a)	PLA	124.8±0.5
	P/M1	55.0±0.3
	P/M3	29.5±0.5
	P/M5	10.6±0.4
	P/M7	6.4±0.5
	P/M9	4.6±0.3
(b)	P/C1	68.7±0.3
	P/C3	50.8±0.5
	P/C5	34.4±0.4
	P/C7	32.8±0.5
	P/C9	30.5±0.3
(c)	P/M5/C1	89.6±0.4
	P/M5/C3	56.8±0.3
	P/M5/C5	37.7±0.5
	P/M5/C7	33.5±0.4
	P/M5/C9	29.4±0.3

Table 3 The 2θ angle and *d*-spacing of MMT, a P/M5 nanocomposite, a P/M5/C1 hybrid nanocomposite and a P/M5/C3 hybrid nanocomposite.

Sample	**MMT**	**P/M5**	**P/M5/C1**	**P/M5/C3**
	001	001	001	001
2θ°	4.15	2.82	2.76	2.94
***d*-spacing(nm)**	2.14	3.15	3.21	3.02

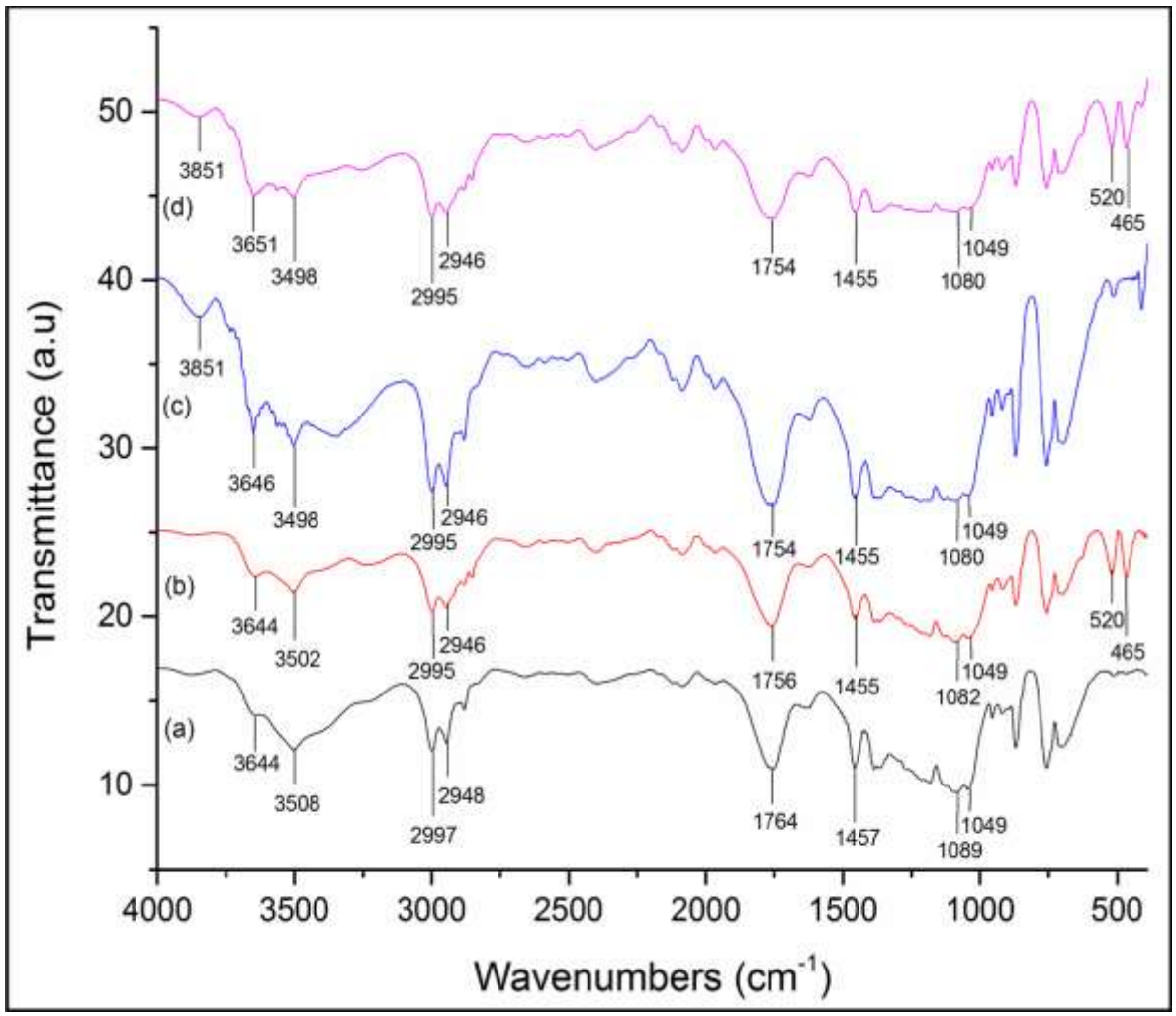
Transmittance (a.u)
Wavenumbers (cm-1)
(d)
3851
3651
3498
2995
2946
1754
1455
1080
1049
520
465
(c)
3851
3646
3498
2995
2946
1754
1455
1080
1049
(b)
3644
3502
2995
2946
1756
1455
1082
1049
520
465
(a)
3644
3508
2997
2948
1764
1457
1089
1049
4000
3500
3000
2500
2000
1500
1000
500
50
40
30
20
10

Fig. 1

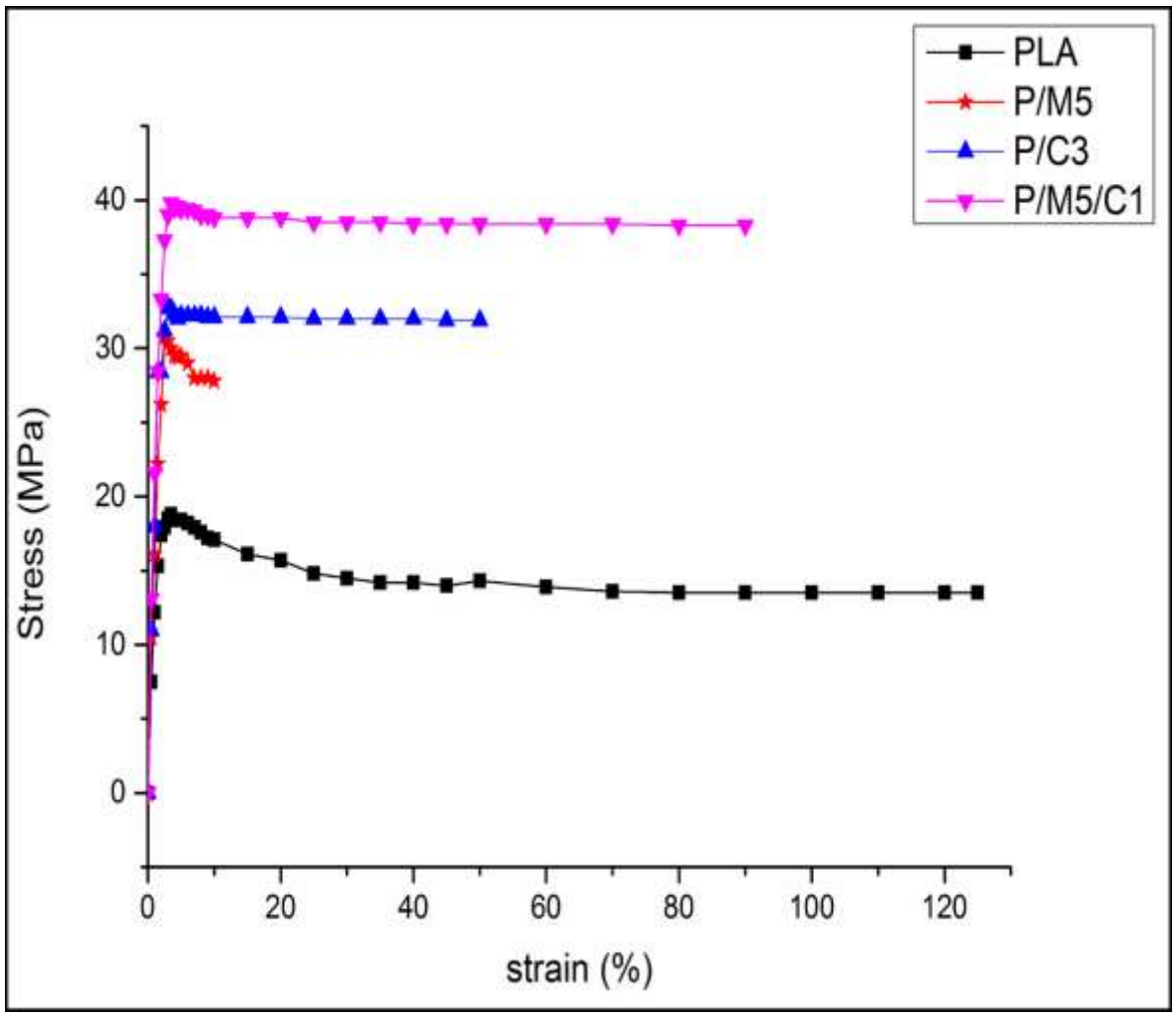
PLA
P/M5
P/C3
P/M5/C1
Stress (MPa)
strain (%)
0
10
20
30
40
0
20
40
60
80
100
120

Fig. 2

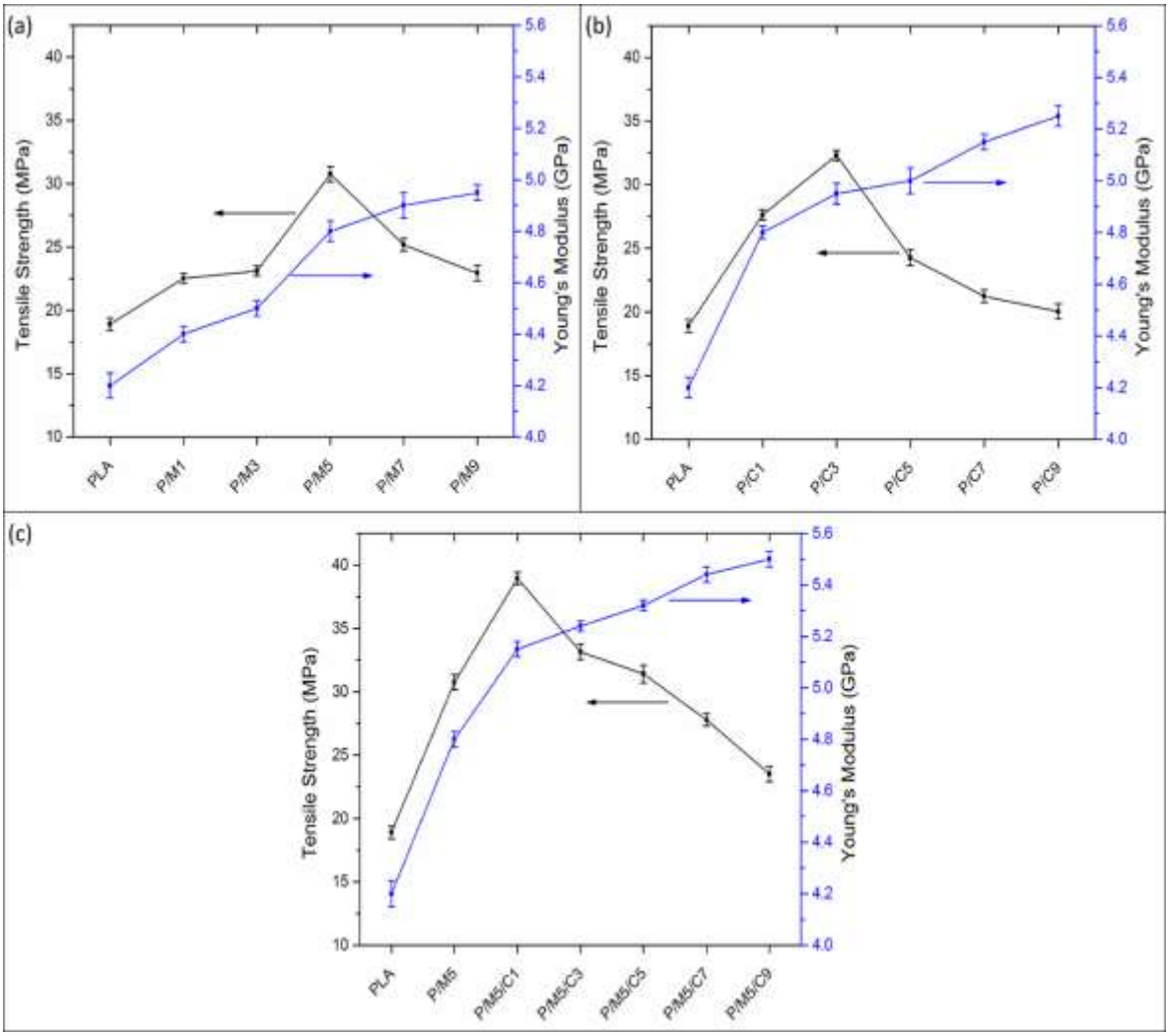
(a)
Tensile Strength (MPa)
Young's Modulus (GPa)
PLA
P/M1
P/M3
P/M5
P/M7
P/M9
(b)
Tensile Strength (MPa)
Young's Modulus (GPa)
PLA
P/C1
P/C3
P/C5
P/C7
P/C9
(c)
Tensile Strength (MPa)
Young's Modulus (GPa)
PLA
P/M5
P/M5/C1
P/M5/C3
P/M5/C5
P/M5/C7
P/M5/C9

Fig. 3

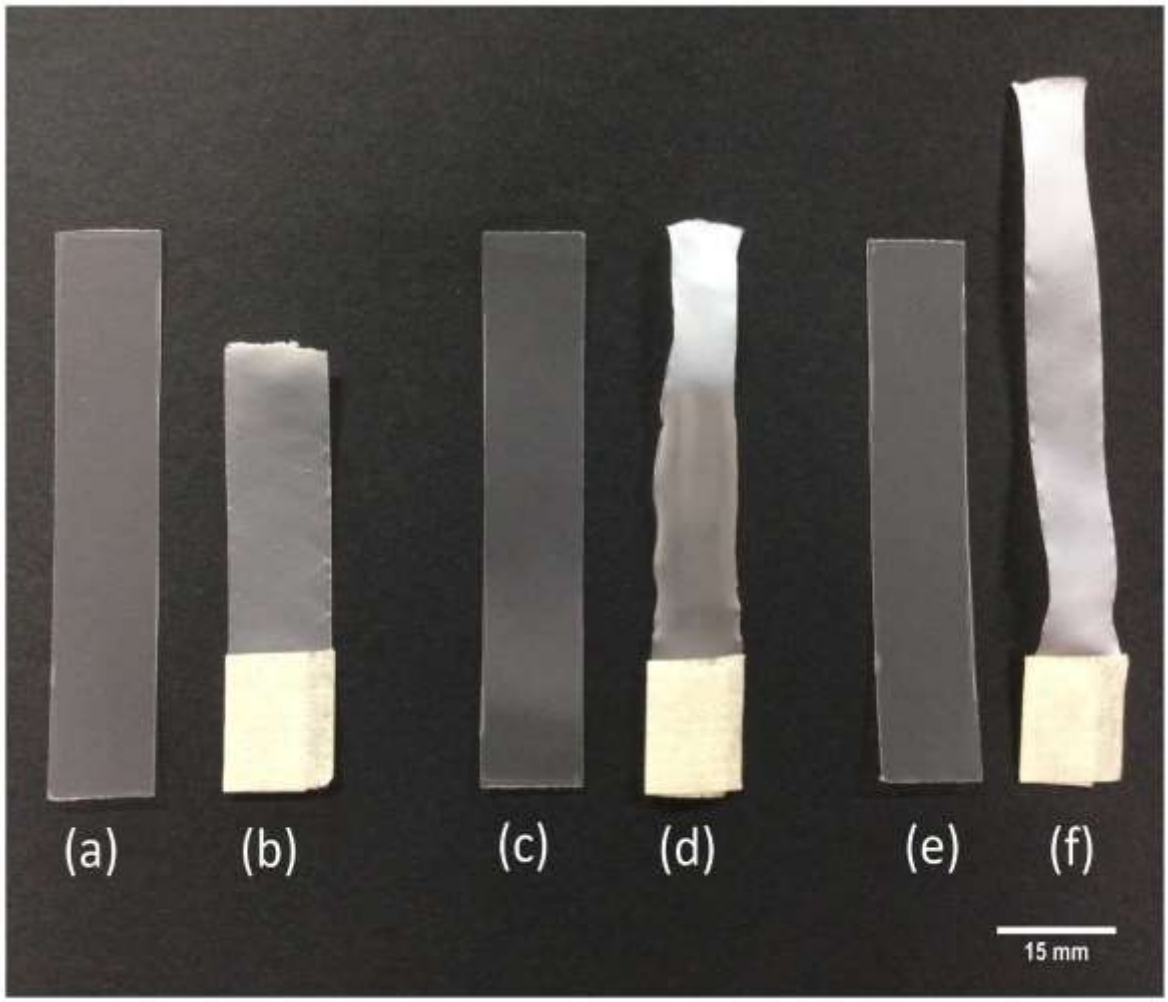

Fig. 4

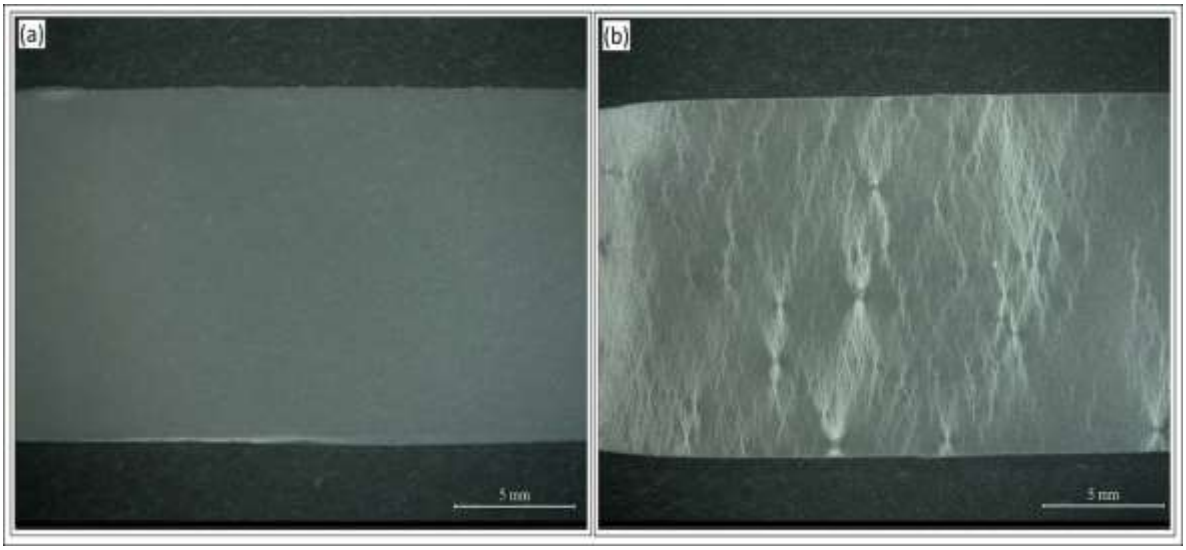

Fig. 5

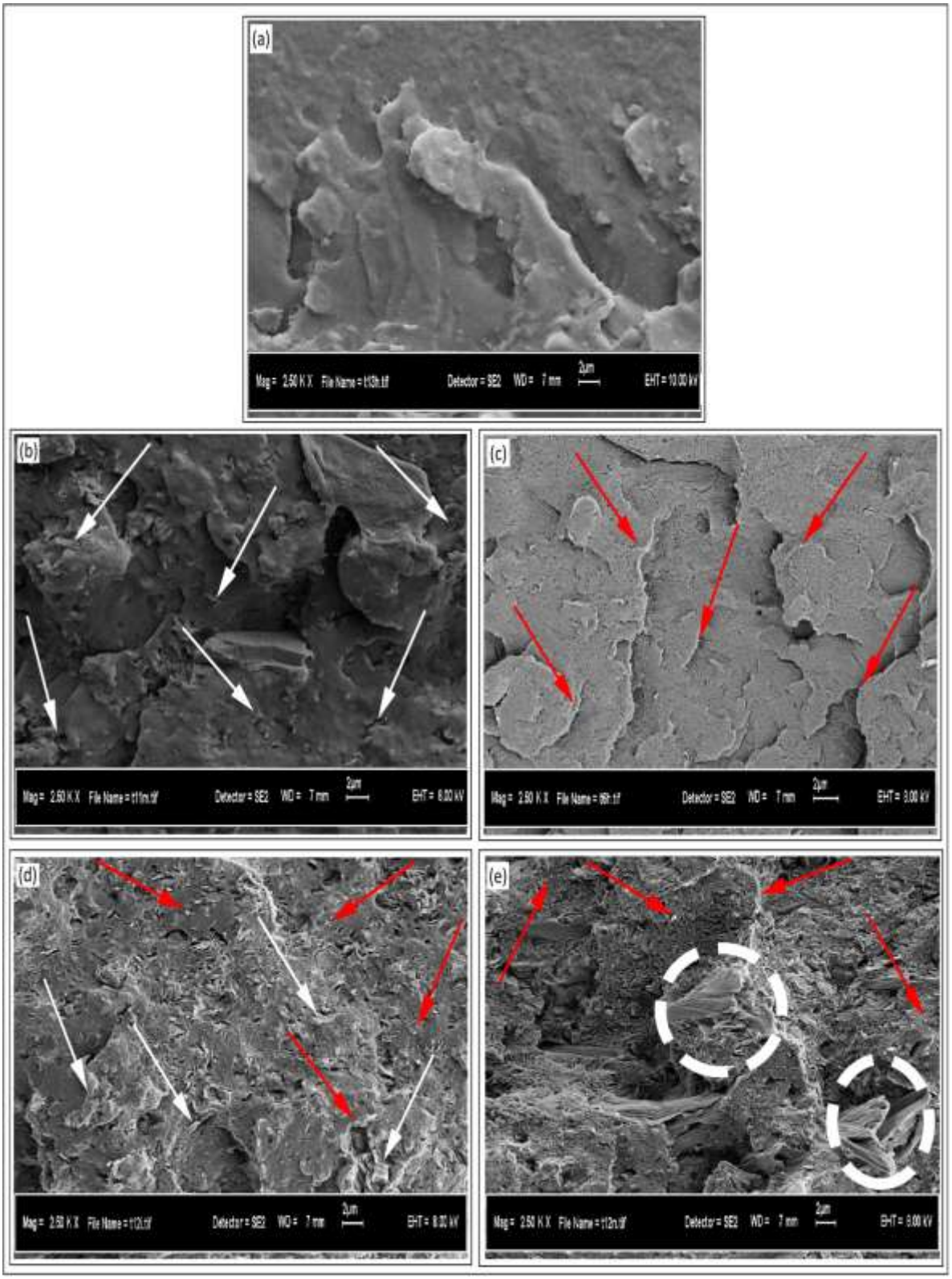

Fig. 6

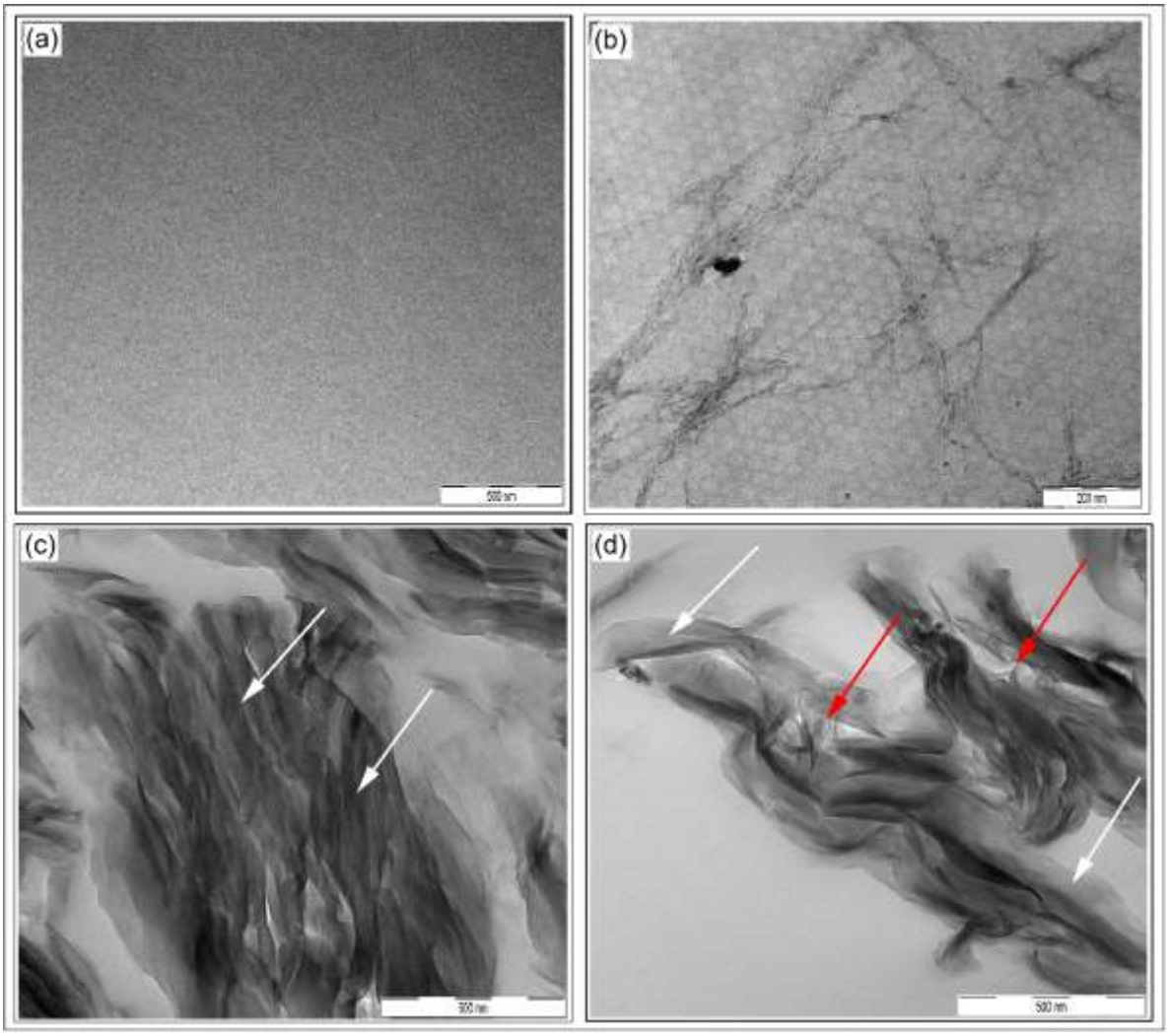

Fig. 7

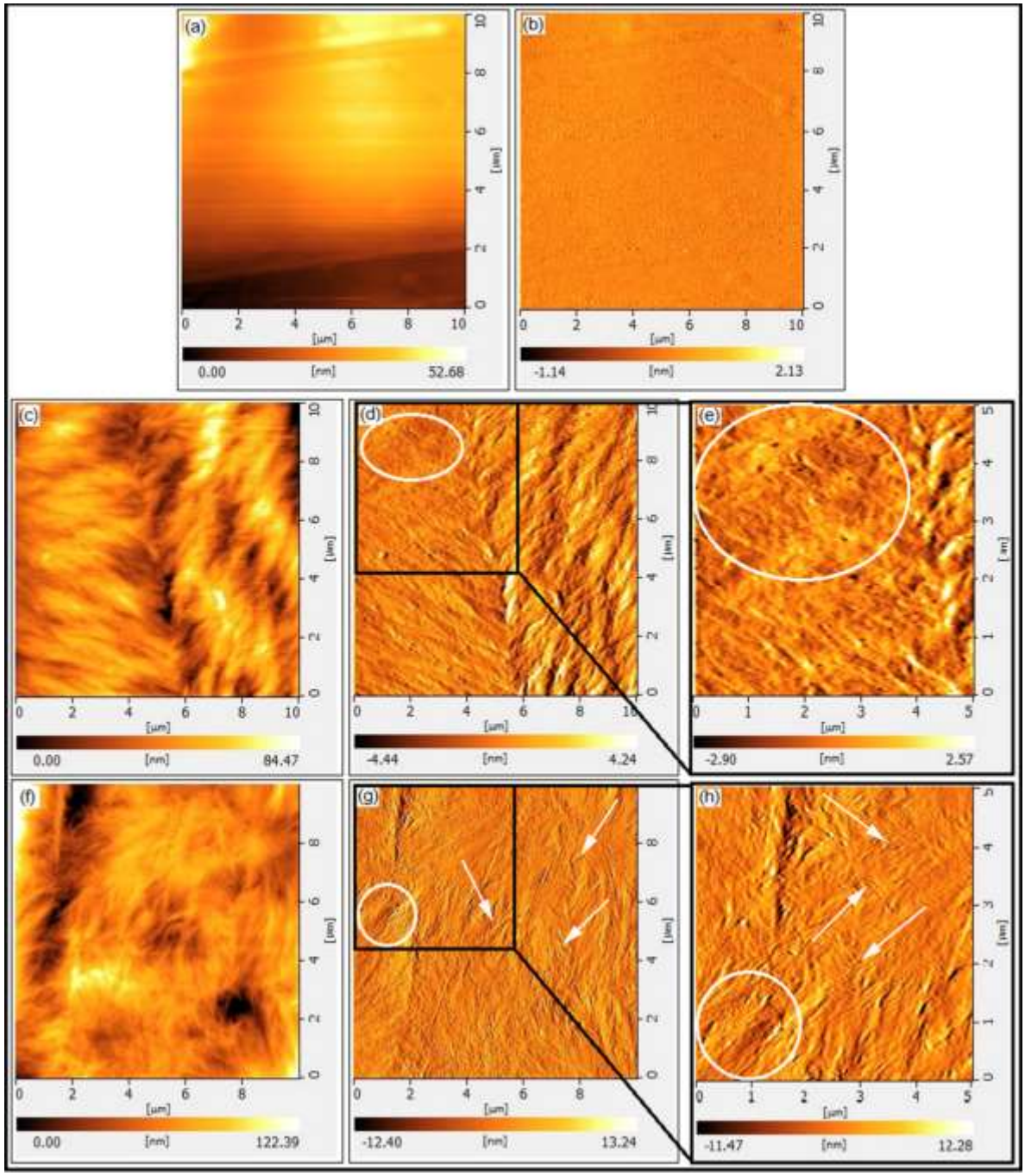
(a)
0.00 [nm] 52.68
(b)
-1.14 [nm] 2.13
(c)
0.00 [nm] 84.47
(d)
-4.44 [nm] 4.24
(e)
-2.90 [nm] 2.57
(f)
0.00 [nm] 122.39
(g)
-12.40 [nm] 13.24
(h)
-11.47 [nm] 12.28
[µm]

Fig. 8

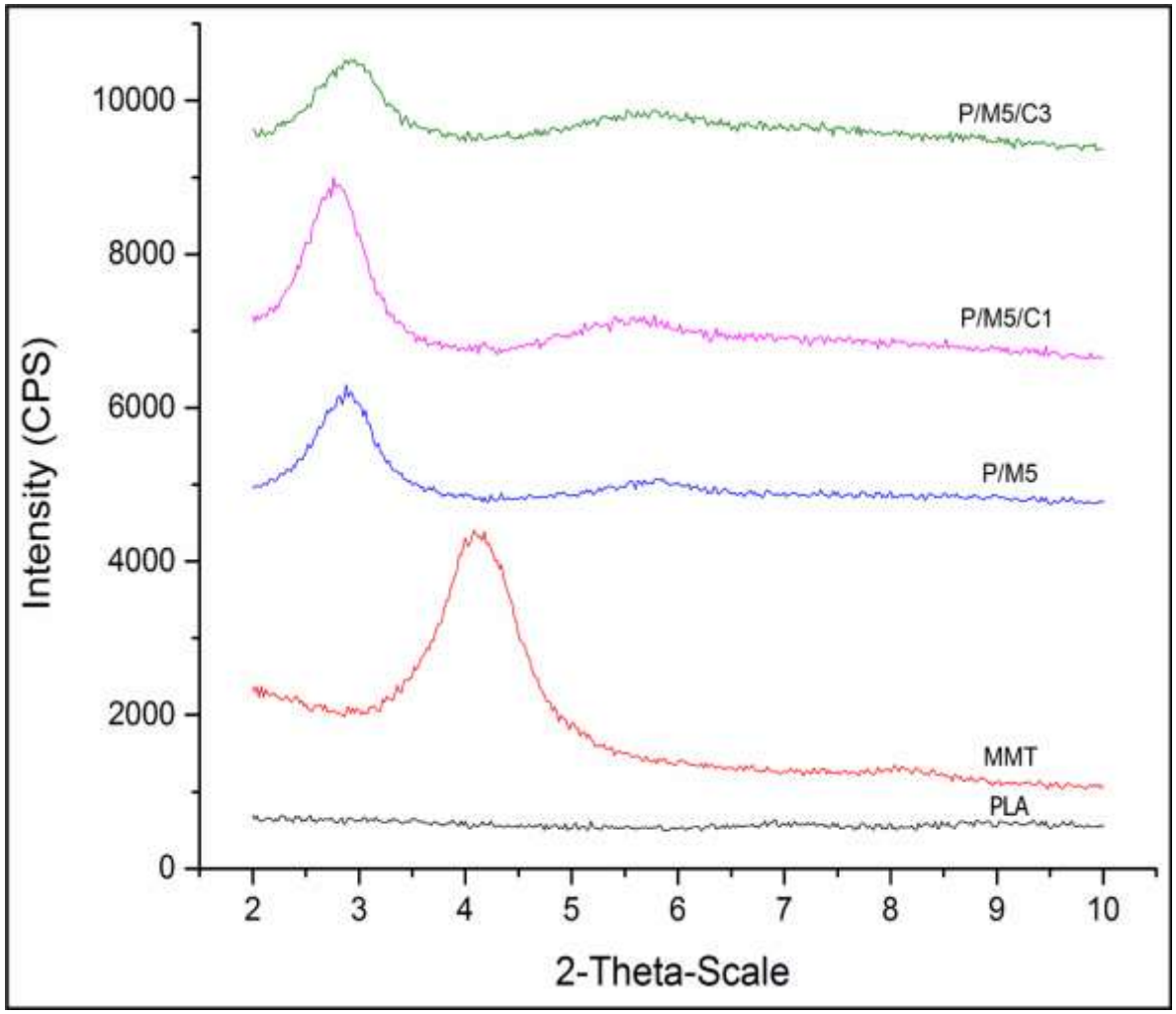
Intensity (CPS)
10000
8000
6000
4000
2000
0
2
3
4
5
6
7
8
9
10
2-Theta-Scale
P/M5/C3
P/M5/C1
P/M5
MMT
PLA

Fig. 9